Journal of Molecular Liquids 427 (2025) 127401

Contents lists available at ScienceDirect

Journal of Molecular Liquids

journal homepage: www.elsevier.com/locate/molliq

A highly chromotropic phenacylated dissymmetric bis-viologen and its base-sensing properties

Valentin Silveira [a], Raffaello Papadakis [a,b,*]

[a] Department of Forest Biomaterials and Technology, Swedish University of Agricultural Sciences, Vallvägen 9C, Uppsala 756 51, Sweden
[b] School of Chemical Engineering, National Technical University of Athens, Athens 15780, Greece

ARTICLE INFO

Keywords:
Viologens
Chromism
Solvent effects
Solvatochromism
Base-sensing properties
Vapochromism

ABSTRACT

The synthesis and drastic chromic properties of a novel phenacyl-substituted bis-viologen are reported. The aforementioned viologen was proved to undergo reversible deprotonation leading to a highly-chromic compound as a result of the pH-dependent activity of the ketone-enolate system that it encompasses. The deprotonation is feasible through inorganic bases such as sodium hydroxide as well as organic bases e.g. diisopropyl ethylamine. The propensity of the viologen to undergo chromic modifications in solution as well as in solid state is examined. In solution, a negative solvatochromic response is observed and for its quantification, a suitable linear solvation energy relationship (LSER) is employed. Finally, the vapochromic response of the title viologen is qualitatively assessed in powder form as well when absorbed on SiO_2 plates.

1. Introduction

Viologens are structurally *N,N*′-disubstituted derivatives of 4,4′-dipyridyl or 2,2′-dipyridyl. In recent years, this widely known class of positively charged heterocycles have found a wide range of applications [1–3]. The applications span from supramolecular chemistry [4–6], and the research fields of molecular machines [7,8] and switches [9–11], to electrochromic materials and devices [12,13], solvatochromic dyes [14,15], and chromotropic sensors and actuators [16–18]. Different kinds of substituents on the two quaternized N-atoms of a viologen shape its properties as it is clear that their redox, optical and chromic properties readily depend on the type of substituents [1]. The idea of introducing active methylene moieties on the quaternary N-atoms of bispyridinium compounds in order to induce viologen-based chromic effects is not new. Indeed, Papadakis and coworkers as early as 2012 reported on the drastic viologen chromotropism activated upon insertion of the phenacyl functional groups on one of the N-atoms of a 4,4′-bipyridine-based viologen [14]. The electron push–pull effect was further examined by altering the substituents on the other N-end of a viologen [14]. The drastic chromotropic behavior was attributed to the formation of an enolate in conjugation to the viologen π-electron system, exhibiting electron deficiency and being capable of stabilizing the negative charge (see Scheme 1). Similar observations were later on made by Hu et al [19].

These attempts fall under the concept of employment of viologen-based or "monoquat" scaffolds as electron acceptors, in conjunction with electron-donating groups like enolates [14,18], ferrocyanide [20–23], and phenolates [18]. The aforementioned approach has in recent years gained widespread acceptance among research groups and serves as a pivotal strategy for creating chromotropic compounds and materials [1].

To the best of the authors' knowledge, dissymmetric 4,4′-dipyridyl-based viologens with chromic properties have been rarely reported to date, and this is presumably associated with the synthetic challenges relating to dissymmetric viologens. In this study, we aim to synthesize and develop a novel viologen of this type with chromic properties. To achieve this, a synthetic approach employing a flexible −xylene bridge connecting two viologen units which were subsequently phenacetylated was adopted (in Scheme 2; compound **8** will be herein referred to as PABV). The choice of connecting group between the viologen units is

Abbreviations: aq, Aqueous (as suffix: e.g. PABVaq); CT, Charge Transfer; conc, Concentrated (as suffix: e.g. NH_4OH_{conc}); DCM, Dichloromethane; DIPEA, *N,N*-diisopropylethylamine; DMF, *N,N*-Dimethylformamide; DMSO, Dimethylsulfoxide; DTG, Derivative Thermogravimetry; FA, formamide; FTIR, Fourier-transform infrared spectroscopy; LSER, Linear Solvation Energy Relationship; NMR, Nuclear Magnetic Resonance; PABV, Compound **8**, Phenacyl *bis*-viologen (1′,1‴-(1,2-phenylenebis(methylene))bis(1-(2-oxo-2-phenylethyl)-[4,4′-bipyridine]-1,1′-diium) tetrabromide; TGA, Thermogravimetric analysis.

* Corresponding author at: Department of Forest Biomaterials and Technology, Swedish University of Agricultural Sciences, Vallvägen 9C, Uppsala 756 51, Sweden (Raffaello Papadakis).

E-mail address: rafail.papadakis@slu.se (R. Papadakis).

https://doi.org/10.1016/j.molliq.2025.127401
Received 3 November 2024; Received in revised form 28 February 2025; Accepted 15 March 2025
Available online 18 March 2025

critical. Notably, a recent report by one of the authors highlighted a bis-viologen with full π-conjugation, utilizing an azobenzene bridge as a chromotropic axial component in a family of [2] rotaxanes [21]. In that context, the bis-viologen serves as an electron-deficient aromatic ligand, capable of accepting two single electrons from the two $Fe^{II}(CN)_5$ endcaps [21,24]. The flexibility that the −xylene bridge introduces is a crucial feature of the structure since there is a clear connection of the flexibility of the bridge and the optical properties of viologens [1]. In addition to synthesizing and characterizing the title viologen, this study examines its behavior under various stimuli, including changes in pH, exposure to dissolved base, organic base vapors, and solvent polarity. A suitable model to quantitatively analyze the solvatochromic properties of the viologen is employed. Furthermore, an experimental approach for qualitatively assessing its vapochromic behavior is presented.

2. Results and discussion

2.1. Synthesis

PABV was synthesized in two steps. Initially, an excess of 4,4′-dipyridyl (corresponding to slightly more than two equivalents) was reacted to one equivalent of *ortho*-xylene dibromide (see Scheme 2). The electrophile was added portion-wise. The reaction took place in anhydrous acetonitrile under reflux conditions. During the reaction, a precipitate was formed, and to ensure that the reaction proceeded to completion, the reaction progress was monitored using thin layer chromatography (TLC). The product was allowed to cool and then was filtered. It was finally isolated/purified through reprecipitation in cold acetone (for details see Materials and Methods section).

In a second step, the non-quaternized nitrogen atoms of the two 4,4′-dipyridyl units are reacted to phenacyl bromide in DMF at 80 °C overnight (Scheme 2). No ion exchange is required since the product as a tetrabromide salt is readily soluble in water as well as a wide range of organic solvents and therefore all the tests on chromotropism were performed on the tetrabromide salt of PABV. In fact, the primary chromic effects are observed in water in contrast to organic solvents. Therefore, exchanging the ions to $(PF_6)^-$ or other forms soluble in organic solvents would hinder testing in water due to the water insolubility of the latter.

2.2. Characterization

PABV was characterized using various analytical methods. ^{1}H NMR analyses clearly confirm the formation of the dissymmetric viologen. Specifically, in the ^{1}H NMR spectrum of PABV the −protons of 4,4′-bipyridinium units appear as the most deshielded protons of the structure. Due to the dissymmetric structure of PABV, the ^{1}H NMR spectrum of PABV involves two doublet signals, one at 9.61–9.59 ppm pertaining to the −4,4′-bipyridine protons adjacent to the −xylene bridge (4H; J = 6.3 Hz) and a second one pertaining to the −4,4′-bipyridine protons adjacent to the phenacyl substituents at 9.40–9.39 ppm (4H; J = 6.3 Hz; see Fig. 1). The *meta*-protons of the 4,4′-dipyridinium units are located closer to one another and as anticipated they are less deshielded compared to −protons 9.01–9.00 ppm and 8.97–8.96 ppm both exhibiting coupling constants of 6.3——6.4 Hz (see Materials and Methods section for details). Moreover, characteristic aromatic signals pertaining to the −xylene bridge and the phenacyl end-caps appear in the region 7.20–8.10 ppm (see Fig. 1). Additionally, the two types of methylene protons present in the structure of PABV exhibit ^{1}H NMR singlet signals at 6.72 ppm (>CH_2 group neighboring to the phenacyl groups) and 6.48 ppm (−xylene > CH_2 groups).

FTIR spectrophotometry confirms the presence of phenacyl groups with a ketonic > C═O stretching band at 1696 cm^{-1} characteristic of a ketone in conjugation to a phenyl ring as well as a band centered at 1449 cm^{-1} corresponding to the bending of ketonic α-CH_2 groups (see Fig. 2). Furthermore, a series of signals pertaining to the aromatic/conjugated system of PABV were identified with a range of C═C stretching bands most characteristic being the 1637 cm^{-1} (aromatic C═C stretching; see Fig. 2). Additionally, a band at and 1558 cm^{-1} corresponding to C═N stretching confirms the presence of pyridinium entities (Fig. 2).

Thermogravimetric analysis indicated that PABV is thermally stable at temperatures up to approximately 220 °C. This is in line with the results obtained through melting point measurements (melting/decomposition at 242 °C). Indeed, heating between 30 and 145 °C resulted in a roughly 14 % mass loss (Fig. 3). This mass loss presumably corresponds to water loss [25] and through that it can be concluded that the product which was obtained after reprecipitation (see Experimental Details), contains approx. 9 water molecules per molecule of PABV. FTIR analysis on a sample thermally treated upon a TGA experiment between 30 and 220 degrees indicated that the structure remains the same as the

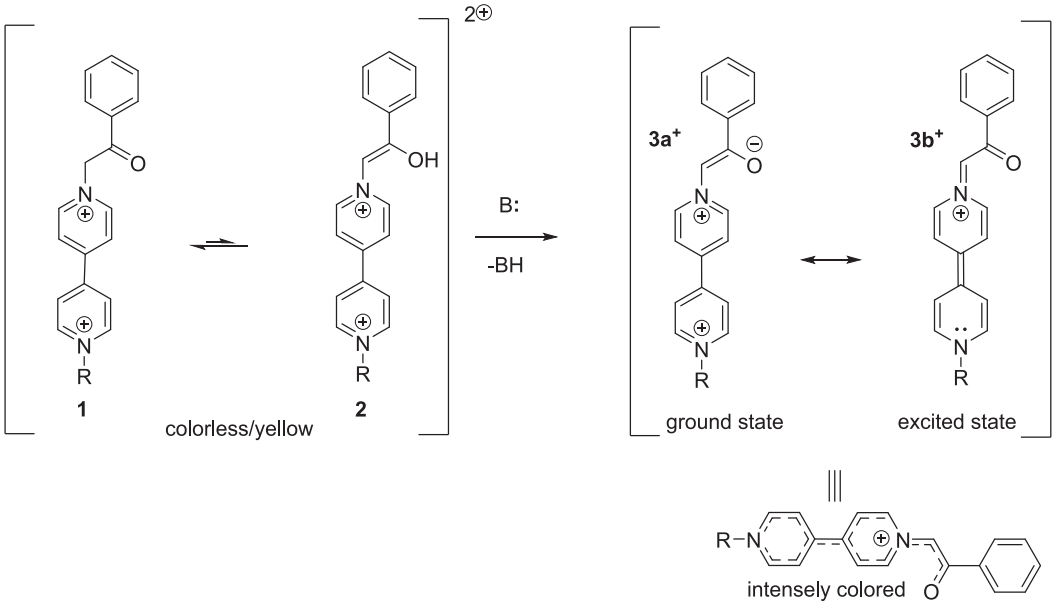

Scheme 1. The effect of deprotonation on the resonance structures of a phenacylated viologen.

starting material; Merely, the OH-stretching bands is reduced as a result of water loss.This information is also in line with the chemical formula $C_{44}H_{38}N_4O_2Br_4{\cdot}9H_2O$ which was confirmed through elemental analysis (see Experimental Details section). Heating above 140 °C and up to 220 °C results in no further mass loss. Nonetheless, heating further above 220 °C lead to structure deterioration. Two main phases were identified during the thermal decomposition of PABV; one between 220 and 250 °C and a second one between 250 and 400 °C. Most likely and based on FTIR analysis after separately heating between 30 and 250 °C the first treatment results in excretion of the phenacyl group. Based on the above information, it can be concluded that PABV can be conveniently used as a sensor (*vide infra*) at temperatures ranging from r.t. and up to 220 °C.

2.3. Chromotropic behavior in solution

PABV has a pronounced sensitivity to both organic and inorganic bases in solution. As seen in the photo of Fig. 4A, while a 1 mM solution of PABV in deionized water has a light yellow color, solutions containing PABV at the same concentration and gradually higher amounts of a base (in case of 4A *N,N*-diisopropylethylamine (DIPEA), also known as the Hünig's base used as a proton scavenger) exhibit intense pink to even violet coloration. Clearly, this effect is associated with the interaction of a base like DIPEA with H-atoms of enolate units of PABV according to Scheme 3. Recently, Papadakis et al. showed that non-symmetric monoviologens bearing phenacyl and aryl units as their *N*-substituents using UV–Vis spectrophotometry and NMR spectrometry [14]. As seen in Fig. 4, PABV is capable of sensing the base.

at concentrations as low as 180 μM (plot of Fig. 4C). The changes in absorbance of the CT band appearing in the electronic spectra of PABV upon addition of DIPEA can be tracked accurately using UV–Vis spectrophotometry (see Fig. 4B). Saturation of the CT-band signal emerging at 528 nm occurs at DIPEA concentrations above 250 μM.

Evidence on the formation of enolates in conjugation to the 4,4′-dipyridyl backbones upon treatment with base is provided through FTIR analysis. Upon treatment of PABV with NaOH (see details in experimental section), the FTIR features of PABV between 800 and 1800 cm^{-1} are drastically influenced (see Fig. 5). First of all, new bands emerged, most important being at 891.3 cm^{-1}, possibly corresponding to out-of-plane bending vibrations of C–H bonds in the substituted vinyl group formed upon deprotonation (see Scheme 3, structure $\mathbf{9}^{4+}$). The band at 1176 cm^{-1} corresponds to a C-O stretching vibration of the formed enol, appearing stronger than prior to deprotonation. Additionally, bands at 1492 cm cm^{-1} and 1582 cm^{-1} corresponding to C═C and C═N stretching vibrations, respectively, associated with changes in the aromatic pyridinium ring upon deprotonation. Other bands of smaller

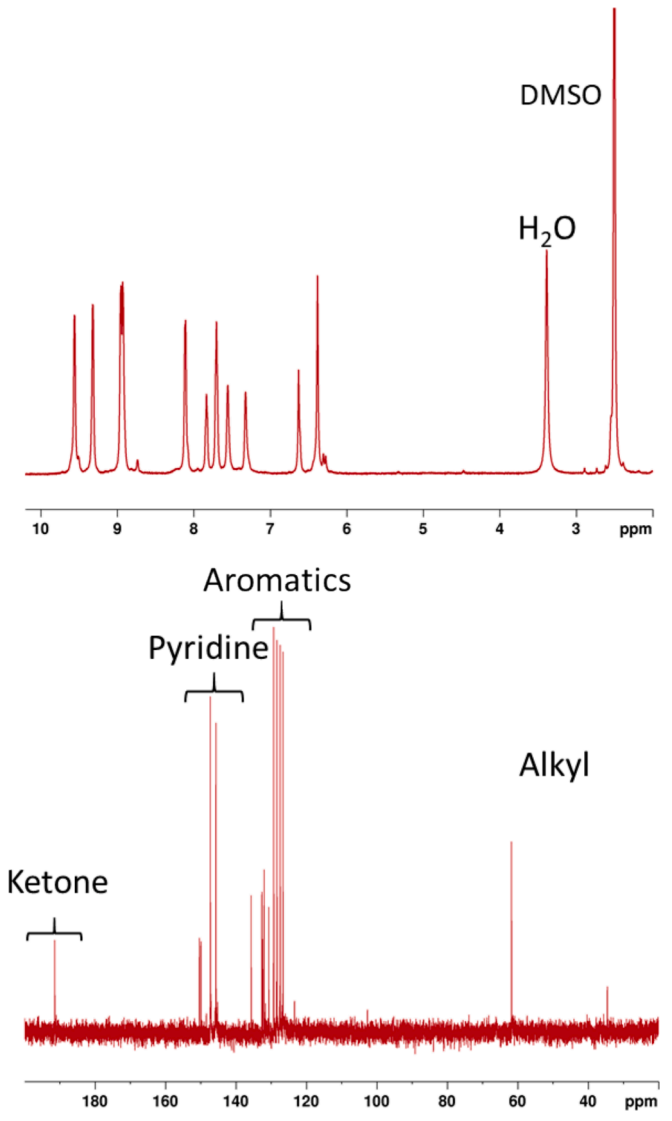

Fig. 1. ^{1}H NMR (upper) and ^{13}C NMR (lower) spectra of PABV recorded in DMSO-d_6 at 25 °C.

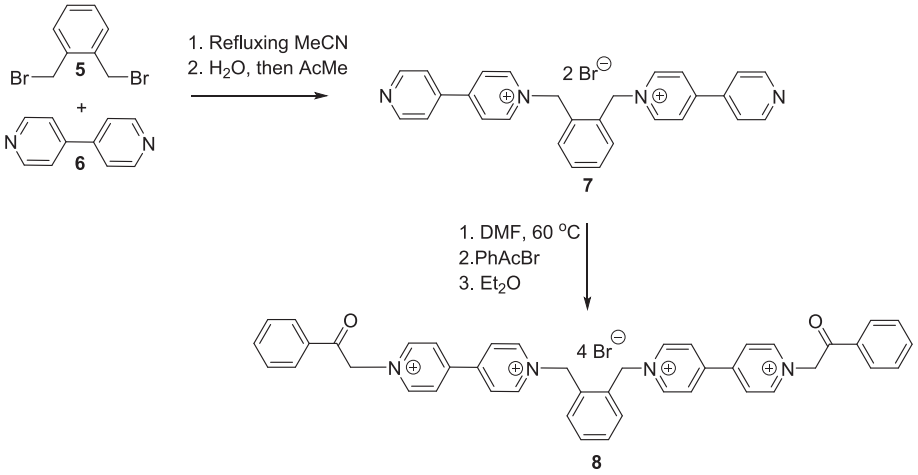

Scheme 2. Synthetic route followed for the production of PABV (**8**).

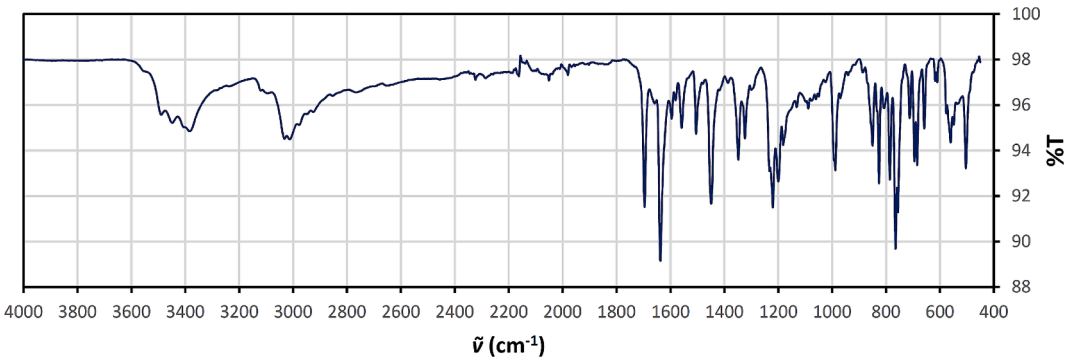

Fig. 2. ATR-FTIR spectra of PABV recorded in the solid state.

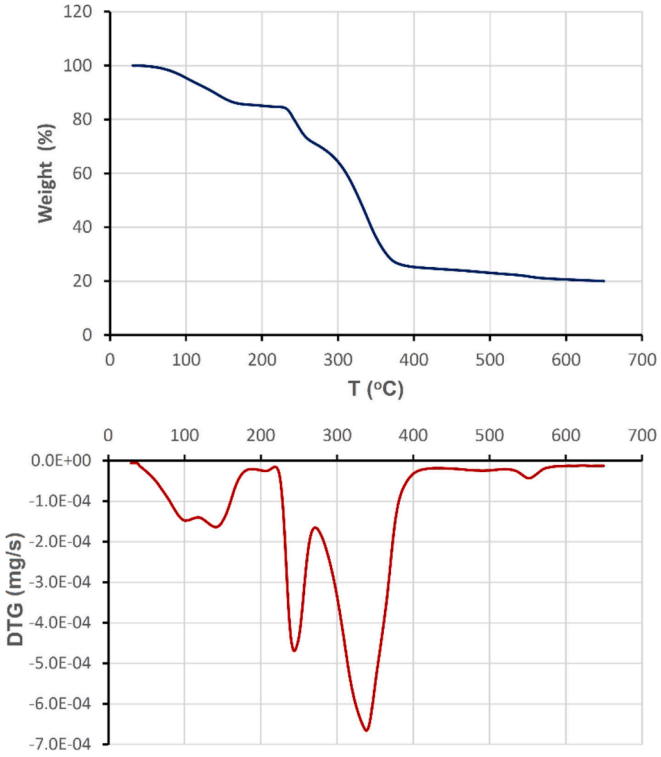

Fig. 3. TGA (A) and DTG (B) thermogram of PABV recorded between 30 and 650 °C.

contribution were also observed e.g. at 1019, 1088, 1302 and 1426 cm^{-1}. Manifestly, the prevailing resonance pattern of PABV changes upon deprotonation, resulting in the donation of electron density from the enolates to the electron-deficient 4,4′-bipyridyl units. As proposed in Scheme 3 and supported by the FTIR findings, the quinoidal pattern becomes more prominent than the aromatic pattern, which prevails in the absence of a base. Specifically, the bands at 1637 cm^{-1} (C═C stretching) and 1696 cm^{-1} (C═O stretching) exhibit a band intensity ratio (C═O)/(C═C) of about 0.6 prior to deprotonation, which decreases to nearly 0.3 after deprotonation. This observation aligns with the assumption of the adaptation of a quinoidal pattern in the deprotonated form.

2.4. Solvatochromism

As already mentioned PABV is readily soluble in water and a wide range of organic solvents. Upon dissolution, the solvents exhibiting significant basicity can hydrogen bond with the enolic hydrogen atoms (see Scheme 4) and the ones of higher basicity can cause deprotonation. A consequence of this specific interaction (or even deprotonation) is the formation of an electron push–pull system which results in a charge transfer (CT) transition band in the visible spectra of PABV. The latter is responsible for the vivid coloration of PABV in solution. The CT band is readily influenced by solvent polarity. As shown in Fig. 6 this behavior is apparent even by naked eye (see Table 1 for numerical results on the solvent effects on CT band).

The energy of CT is strongly dependent on the polarity of the medium. Solvents of high basicity (either hydrogen bond accepting (HBA) basicity or Lewis basicity) such as acetonitrile or DMSO can interact strongly with the PABV (see Scheme 3). It is easily witnessed that drastic shifts of the CT absorption band of PABV can be induced by different solvents (Fig. 7).

A good way to rationalize the effect of solvent polarity on the electronic spectra of PABV is by use of solvent polarity parameters. Plotting the measured CT energies (see Table 1) against parameter $E_T(30)$ (Reichardt's polarity scale [27]) results in a line with positive slope ($a = 4.741$) and a fairly high correlation coefficient ($r^2 = 0.872$; see Fig. 8)). The positive slope is indicative of a negative solvatochromic effect since it signifies bathochromic shifts (lowering of CT energy) while decreasing $E_T(30)$. It is important to mention that $E_T(30)$ constitutes an empirical measure of solvent dipolarity/polarizability [28]. On the other hand, plotting the measured CT energies of PABV against a parameter expressing solvent Lewis basicity such as *DN* (Gutman's Donor Number) [29] results in a line of negative slope ($\beta = -2.919$; see Fig. 8). This suggests that enhancing the basicity of the solvent leads to higher charge transfer energies. Specifically, solvents with greater ability to form hydrogen bonds with the enolic hydrogen atom or to induce deprotonation (as shown in Scheme 3) tend to stabilize the ground state more effectively. In the electronic ground state, the resonance structure of type **3a** is pronounced, whereas in the excited state (as depicted in Scheme 1), structure **3b** dominates. The observed trend is illustrated by a line with a negative slope in Fig. 8a. Nonetheless, the correlation coefficient involving *DN* was significantly lower than in case of parameter $E_T(30)$. This could imply that solvent dipolarity and polarizability of the medium demonstrates a more important effect on the solvatochromism of PABV than solvent basicity. In order to assess this, a linear solvation energy relationship (LSER) involving both the aforementioned solvent polarity parameters was employed (Eq. (1))

$$E_{CT} = E_{CT,0} + a \bullet \boldsymbol{E_T}(30) + \beta \bullet \boldsymbol{DN} \quad (1)$$

Eq. (1) corresponds to Krygowski-Fawcett equation [30], an LSER which in its original version involves two parameters namely Reichardt's polarity scale $E_T(30)$ and Gutman's donor number (*DN*) [30]. As $E_T(30)$ expresses a mix of solvent Lewis acidity and dipolarity/polarizability and Lewis acidity whereas DN expresses solvent Lewis basicity, the model can be considered as a complete approach simultaneously taking into account specific and non-specific solvent effects. Noteworthy, Papadakis *et al.* have recently successfully employed the same model in its solute and indicator centric form to assess solvent effects occuring in

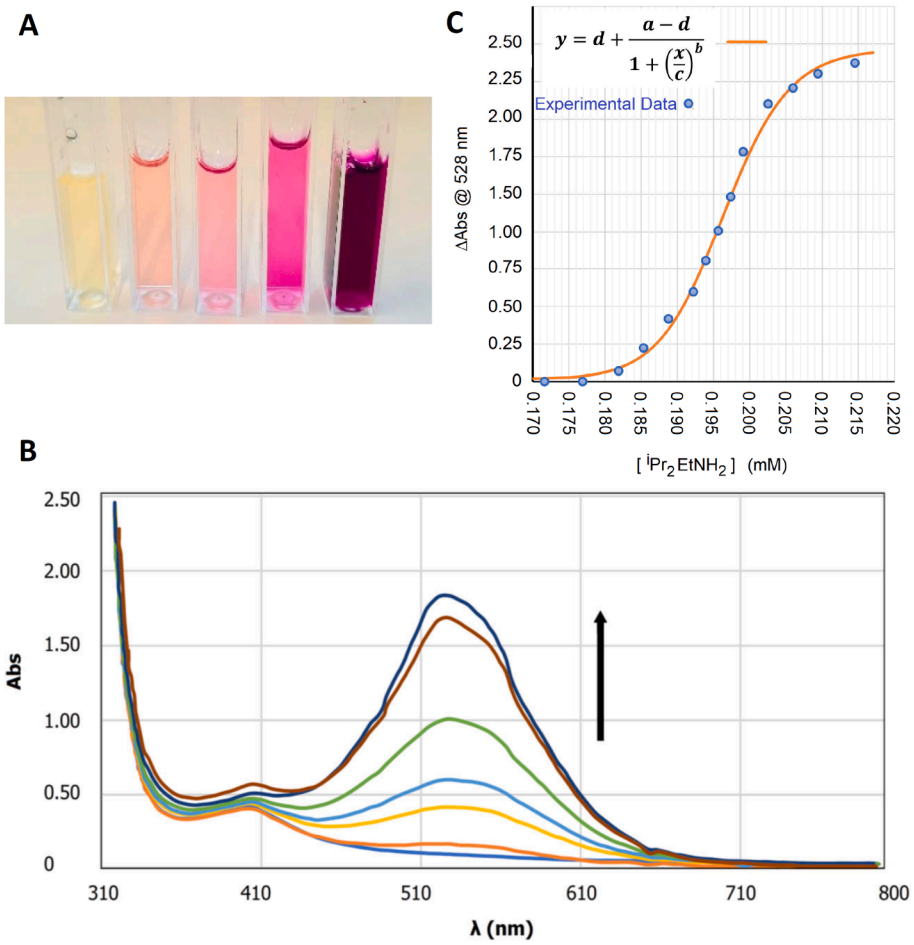

Fig. 4. A) Photo depicting the effect of base (DIPEA) concentration on the color of an aqueous solution of PABV (1 mM). Concentration of DIPEA from left to right: 0.000, 0.180, 0.185, 0.195, 0.215 mM. B) visible spectra of aqueous PABV solution (blue line) and solutions increasing base (DIPEA) concentration from 0.180 to 0.215 mM. C) Plot of $\Delta Abs@528nm$ against the concentration of DIPEA. ($\Delta Abs@528nm$ corresponds to the difference of measured absorbance at 528 nm with respect to aqueous PABV solution without base; [PABV] = 1 mM). Sigmoidal curve obtained through regression analysis [26] (orange line) experimental data appear as blue dots. Sigmoidal fitting equation: y = d + [(a-d)/(1+(x/c)b]; a = 0.0143 ± 0.0499, b = 43.55 ± 5.201, C=0.1964 ± 0.0005, d = 2.219 ± 0.097; $r^2 = 0.9961$. (For interpretation of the references to color in this figure legend, the reader is referred to the web version of this article.)

solvent mixtures [31]. Biparametric linear regression on the spectrally obtained CT energies of PABV against parameters $E_T(30)$ and *DN* resulted in equation (2) which is characteristic of the solvatochromism of PABV.

$$\boldsymbol{E_{CT}}\left(\frac{\boldsymbol{kcal}}{\boldsymbol{mol}}\right) = 41.07 + 0.2039 \bullet \boldsymbol{E_T}(30) - 0.01326 \bullet \boldsymbol{DN}, r^2 = 0.9188 \quad (2)$$

Noteworthy, acetonitrile was excluded from this regression analysis because its coloration may be due to decomposition, through solvolysis of the viologen, rather than a solvatochromic shift.

The success of Eq. (2) in predicting CT energies is reflected in the 3D-plot of Fig. 9 depicting the experimental data with respect to the regression plane obtained through Eq.2.

Additionally, through the statistical analysis it was found that $E_T(30)$ contributes more than *DN* to the observed solvatochromic phenomenon. This finding illustrates that while Lewis/HBA basicity is an important property of a solvent without which the chromic behaviour of PABV could not be triggered, dipolarity and polarizability as expressed through $E_T(30)$ is the driving force shaping the solvatochromic properties of PABV. This is in line with the results of the linear regression performed separately for parameters $E_T(30)$ and *DN* where, as mentioned the correlation coefficient of the $E_{CT} \propto DN$ was significantly lower than that of the correlation: $E_{CT} \propto E_T(30)$.

Based on these findings, it is apparent that PABV is a potent solvatochromic probe of high solvatochromic intensity (i.e. large solvatochromic shifts induced through defined solvent polarity changes). It is noteworthy that the difference between the two extreme recorded cases of solvents/solvent mixtures in terms of solvent dipolarity studied in this work [namely water/AcMe mix. 30:1 v/v (or H/A for short) and neat DMSO] the recorded difference in charge tansfer energy was $\Delta^{H/A}_{DMSO}(E_{CT}) = -3.26 \frac{kcal}{mol}$ corresponding to a $\Delta^{H/A}_{DMSO}(\lambda_{CT}) = +34nm$. The aforementioned recorded difference between these two solvents/solvent mixtures corresponds to a very slight positive change in Lewis/HBA basicity $\left(\Delta^{H/A}_{DMSO}(DN) = 12.1 \frac{kcal}{mol}\right)$ however to a drastic negative change in dipolarity $\left(\Delta^{H/A}_{DMSO}(E_T(30)) = -18.0 \frac{kcal}{mol}\right)$. These findings underline the impact of dipolarity of the medium on the CT-transition of PABV.

Based on the above analysis it is apparent that substantial solvent basicity is required in order to induce a solvatochromic effect on PABV. Water exhibits a *DN* of 17.8 $\frac{kcal}{mol}$ yet by itself it is not possible to induce any chromic effect (the color of PABV aqueous solution in Milli-Q water is light yellow; see inset of Fig. 10). Nonetheless, small amounts of better Lewis bases/solvents such as AcMe or ^{n}BuOH are capable of inducing chromic effects in water (see for instance the case of mixtures HOH/AcMe, 30:1 (v/v) and HOH/nBuOH, 30:1 (v/v). Moreover, it is astonishing that while Milli-Q (0.048 μS/cm, pH = 6.99) water keeps PABV

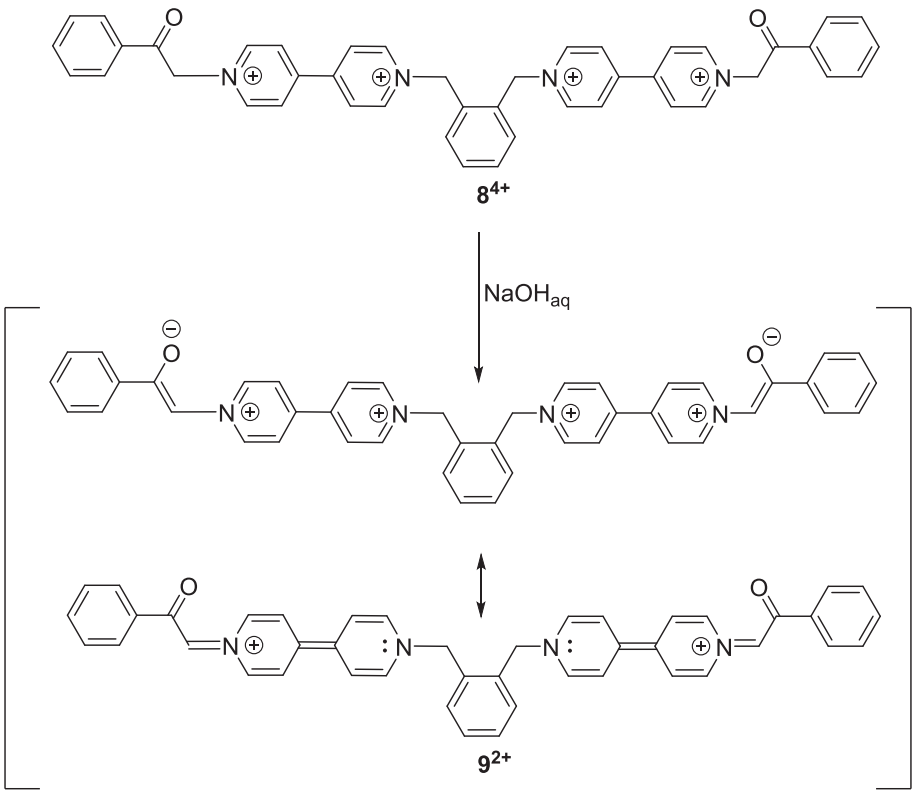

Scheme 3. Deprotonation of PABV using a strong base (NaOH) and corresponding limiting resonance structures of the as formed compound **9.**

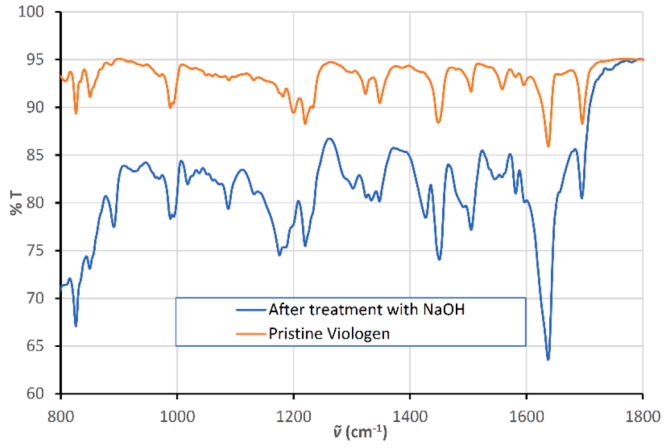

Fig. 5. Partial ATR-FTIR spectrum of pristine PABV (orange line) and PABV after treatment with NaOH(aq) (see Experimental Details). (For interpretation of the references to color in this figure legend, the reader is referred to the web version of this article.)

predominantly in its tetranionic form (yellow color), tap water (pH = 8.4) redners it violet (see Fig. 10). This effect clearly indicates the propensity of PABV to undergo chromism even at traces of base e.g. OH^-. The λ_{max} of a solution of PABV in tap-water was deterimined to be equal to 528 nm. This value is very close to the recorded ones in case of the water-based mixtures HOH/AcMe 30:1 (530 nm) and HOH/nBuOH 30:1 (530 nm) (see details in Table 1). They are also very close to the λ_{max} recorded in water/DIPEA mixtures (528 nm; see Fig. 4B). These facts indicate that the mechanism of this chromic effect is likely associated to deprotonation occuring at pH 8.4 (tap water).

2.5. Vapochromism of PABV in the solid state

The chromotropic behavior of PABV can be also efficiently triggered in the solid state. Specifically, vapochromic responses are observed when powder samples of PABV are exposed to vapors of a volatile amine such as aqueous ammonia or a volatile organic amine e.g. triethylamine. In the photos of Fig. 11 a drastic change of the PABV powder color from yellow to purple is observed upon exposure to ammonia vapors (see experimental details in Fig. 11 and Materials and methods section). These results indicate a drastic vapochromic response even in the powder form. What is noteworthy is that the powder changed color from yellow to violet even after exposure to ammonia vapor for 15 min and moreover after exposure for 1 h, no traces of yellow particles were detected. As a further example of a real sensor application, a message was written on a TLC plate using an aqueous solution of PABV. An interesting effect observed after drying the TLC plate, is the light brown coloration of SiO_2 particles (see Fig. 12); for details on the experiment see Materials and Methods section) which presumably is a result of the PABV with SiO_2. The vapochromic effect was immediate when the dried TLC plate was placed above a beaker containing a small amount of NH_4OH_{conc}. Due to the fluorescence of PABV it is very easy to read the message merely using a black-light source (λ_{em} = 395 nm) as seen in Fig. 12b prior to exposure. These results indicate the potentials of PABV as a vapochromic sensor of basic vapors.

To assess the reversibility of vapochromism, experiments were conducted on SiO_2-TLC plates where compound **8** was absorbed (see Experimental Details). Coloration was induced by exposing the plates to ammonia vapors and subsequently reversed by exposing them to HCl vapors. This process was repeated five times. It was found that minimal changes in color intensity were observed upon repeated coloration/discoloration cycles (5 in total; see Fig. 12D–E). The system demonstrated complete reversibility with no apparent degradation for at least five cycles.

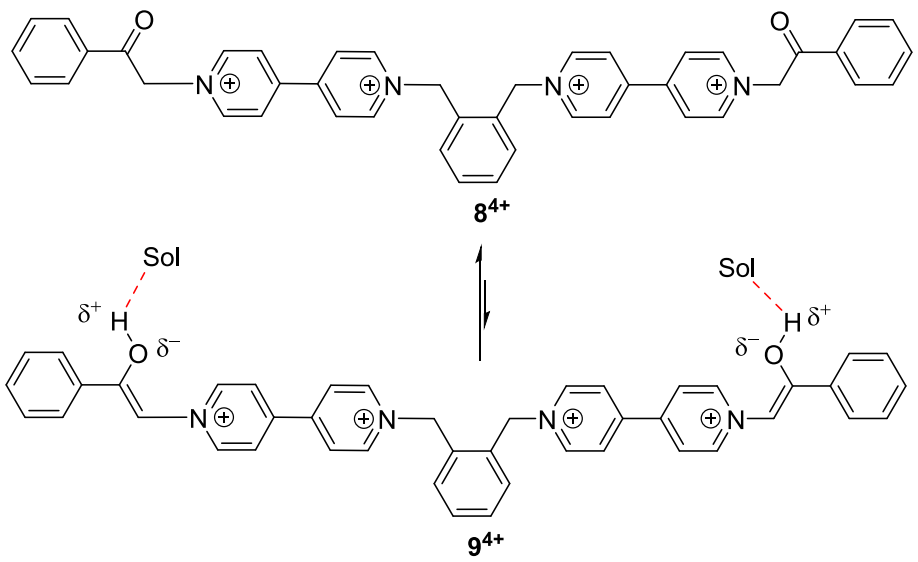

Scheme 4. The specific interaction influencing the solvatochromism of PABV. "Sol" stands for solvent or a generic HBA-base.

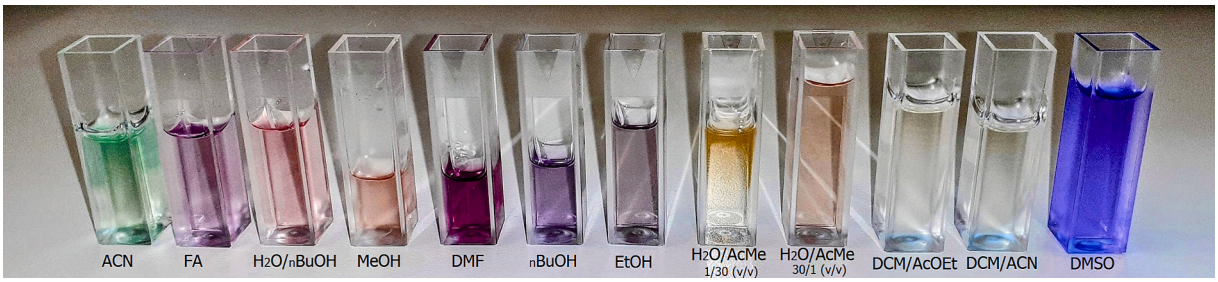

Fig. 6. Photo depicting UV–Vis spectrophotometry cuvettes containing PABV dissolved in a variety of solvents/solvent mixtures.

Table 1
Maximum absorbance CT-wavelengths and corresponding CT wavenumbers and energies of PABV recorded in ten solvents/solvent mixtures along with corresponding solvent polarity parameters E_T **(30)** and ***DN***.

Solvent	λ (nm)	*Annotation*	$\tilde{\nu}$ (cm^{-1})	E_{CT} (kcal/mol)	$E_T(30)^{\spadesuit}$ (kcal/mol)	$DN^{\dagger}$ (kcal/mol)
HOH/AcMe 30:1 (v/v)	530	Lλ■	18,867.9	53.95	63.1	17.8 [32]
HOH/nBuOH 30:1 (v/v)	530	Lλ	18,867.9	53.95	62.7	18.2 [32]
FA	554	Lλ	18,050.5	51.61	55.8	24.8
MeOH	550	Lλ	18,181.8	51.98	55.4	19.0
EtOH	564	Lλ	17,730.5	50.69	51.9	31.4
^{n}BuOH	562	Lλ	17,793.6	50.87	49.7	19.4
MeCN	588	Sλ ‡	17,006.8‡	48.62	45.6	14.0
DMSO	564	Lλ	17,730.5	50.69	45.1	29.9
DMF	564	Lλ	17,730.5	50.69	43.2	26.8
DCM:AcOEt: MeCN:DMF 2:2:1:1drop (v/v/v/v)	578	Lλ	17,301.0	49.47	42.6*	10.1

*Determined directly using Reichardt's solvatochromic betaine.
■ Annotation **Lλ** corresponds to the visible absorption band (wavelength range (450–750 nm) of PABV.
♠ Data from Ref. [28] or otherwise indicated.
† Data from Ref. [29] or otherwise indicated.
‡ Value based on the shorter wavelength (Sλ) UV–Vis band since Lλ likely corresponds to a solvolysis/decomposition product.

2.6. Color stability in liquid and solid state

To assess the color stability in solution, UV–Vis spectrophotometric experiments were performed in DMSO and DMF, two solvents of different polarity. The absorbance of the charge transfer (CT) maxima wavelengths (λ_{max}) of the viologen was recorded at various time points to monitor color stability over time. The results indicated that the color remained stable for several hours with slightly higher stability in DMSO than DMF (see Fig. 13). The experiments were conducted in the presence of air which indicates very high stability. Although there is no evidence of oxidation, it is likely that CO_2 absorption in the liquid state leads to slight acidification, resulting in a slow loss of color through the protonation of the enolate (see Scheme 3). Solvents/media that can better buffer the acid-base equilibria can provide stabilization to the enolates and thus help maintain the stability of the absorbance features. Specific interactions between the solvent and the viologen, such as hydrogen bonding, polarity, and solvent acidity/basicity, play a crucial role in dictating the stability of these absorbance features. Additionally, in more viscous solvents, the diffusion of CO_2 from the air is slower. Therefore, in more viscous solvents, one can expect slower discoloration and higher stability for the enolates of compound **8**. For instance, this is apparent through the comparison of DMSO (viscosity 1.996 cP at 20 °C) and DMF (viscosity 0.799 cP at 20 °C) [33] as shown in Fig. 13.

2.7. Computational details

All correlations presented in this study were performed on *R* (version 4.0.2). The multiparametric model (normalized Krygowski-Fawcet) was employed in order to assess the relative contribution of various

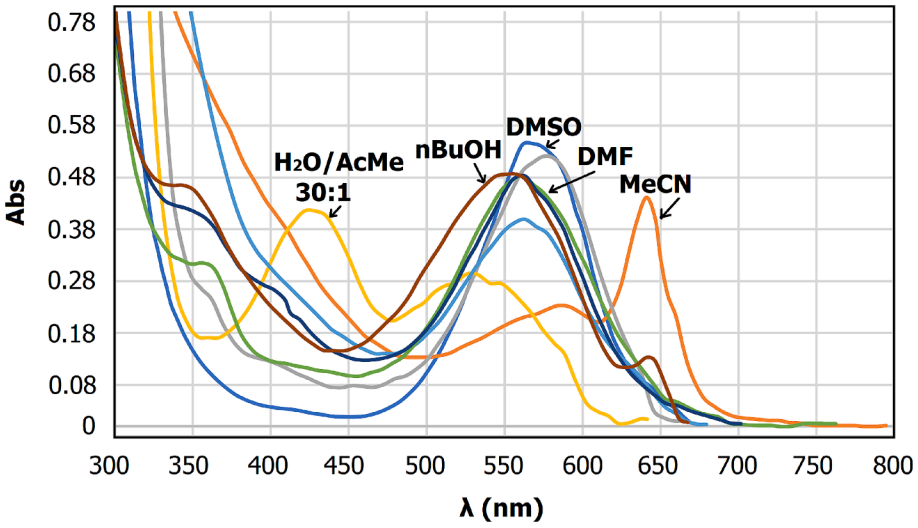

Fig. 7. Visible spectra of PABV recorded in various solvents and solvent mixtures.

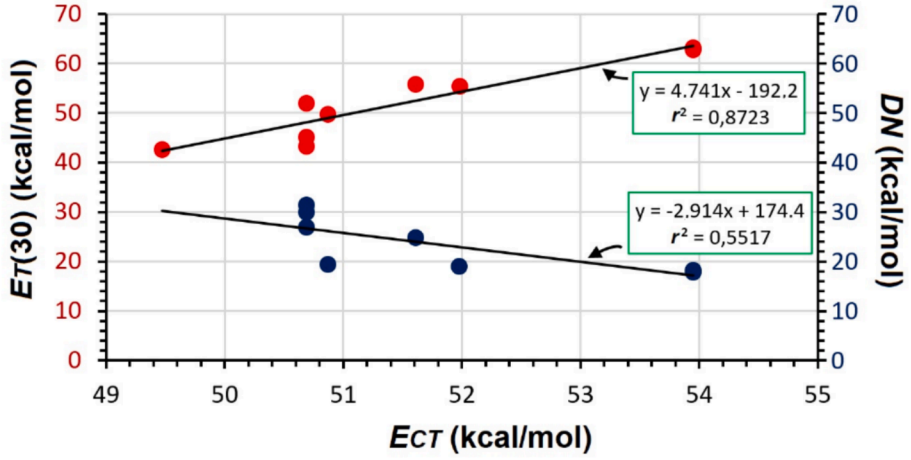

Fig. 8. Plots corresponding to the linear correlations of E_{CT} energies determined for PABV with solvent parameters $E_T(30)$ and *DN*.

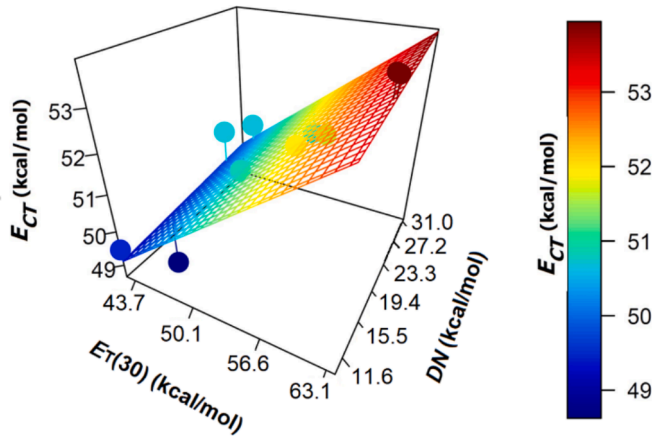

Fig. 9. 3D-Plot depicting the E_{CT} energies experimental data with respect to the regression plane obtained through Eq. (2).

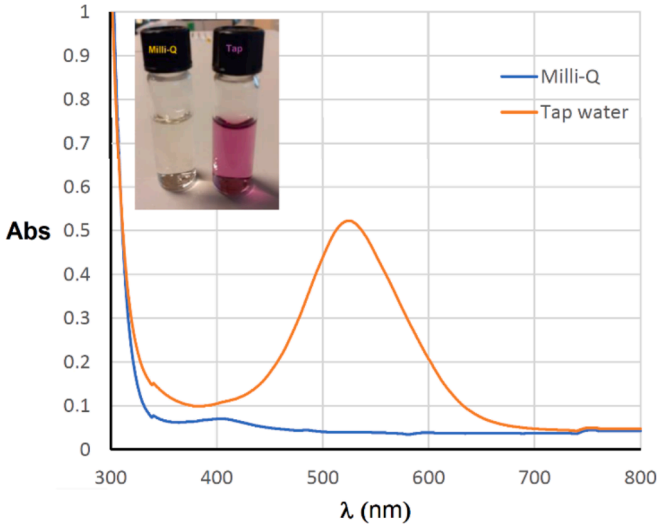

Fig. 10. UV–Vis spectrum of PABV recorded in Milli-Q water and in tap water (pH = 8.4). Inset: photo of the two solutions (Milli-Q on the left, Tap water on the right).

solvatochromic parameters expressing solvent polarity. For the sigmoidal fits, the flowing model was used: $y = d + \frac{a-d}{1+(x/c)^b}$ where y corresponds to the spectrally determined $\Delta Abs@528nm$ and x is the

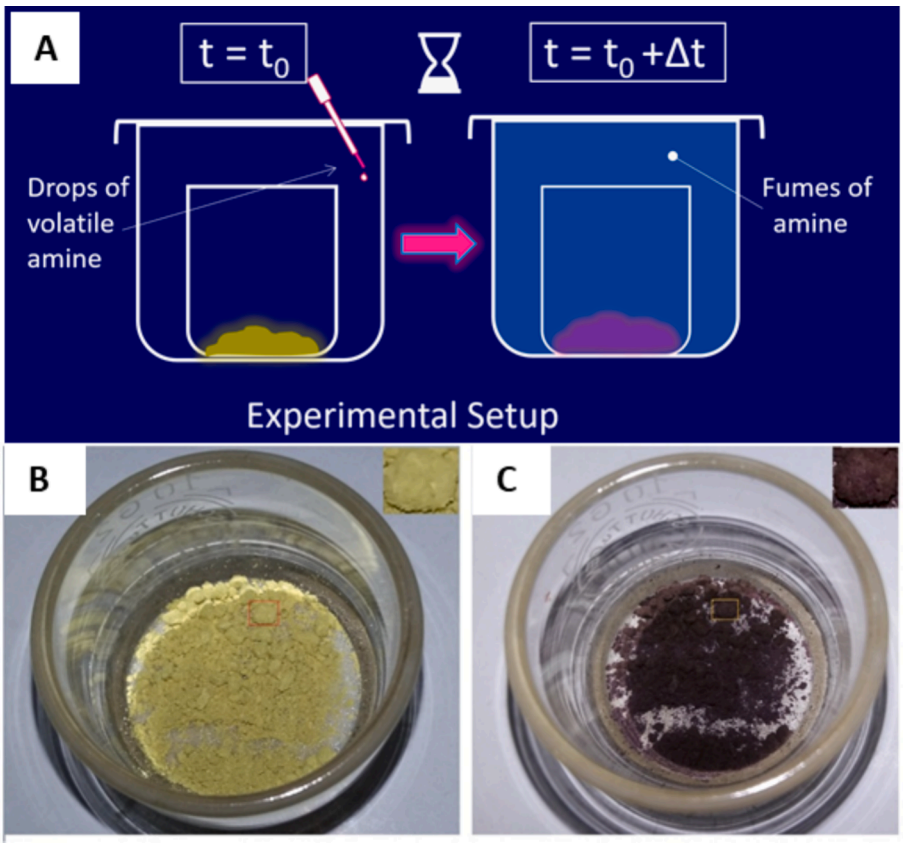

Fig. 11. A) Illustration of the experimental setup used for the vapochromic test applied on powder of PABV B) Photo of the powder of PABV prior to exposure to ammonia vapors and C) Photo after exposure for 15 min.

concentration of base (DIPEA) in mM.

3. Experimental details

3.1. Materials

Compounds 4,4′-bipyridine, phenacetyl bromide, 1,2-bis(bromomethyl)benzene, Acetone (AcMe) all of reagent quality and all solvents (*pro analysis* quality) in this study were purchased from Sigma Aldrich. Solvents were purified according to published procedures prior to use [34]. TLC plates: (Silica Gel on TLC Plates 5 cm × 10 cm) were purchased from Sigma Aldrich.

3.2. Analytical methods

All NMR spectra were recorded a Bruker 500 MHz spectrometer (Bruker Advance Neo, TXO probe), (NMR Center Uppsala). All chemical shifts are presented in ppm and were indirectly referenced to the TMS signal ($\delta = 0.00$ ppm) for proton and carbon using the residual deuterated solvent signal. Elemental Analyses were performed on a Perkin-Elmer Elemental Analyser 2400 CHN. UV–Vis spectra were recorded using a Varian CARY 1E UV–Vis spectrophotometer. Regarding the solvatochromism of compound **4**, typically solutions with a concentration of 750 ppm (approx. 1 mM) were prepared right before any measurement, and measured at 25 ± 1 °C. Each measurement was repeated three times; therefore, each of the values of CT energies listed in Table 1 correspond to the average of three measurements (standard deviation 0.5 nm). Melting points were determined with a Gallenkamp MFB-595 melting point apparatus. Fourier-transform infrared spectroscopy: Infrared spectrum were recorded using a Fourier-transform infrared spectrophotometer (Spectrum Two, Perkin-Elmer, Llantrisant, UK) equipped with a Universal Attenuated Total Reflectance diamond. All FTIR spectra were collected at a spectrum resolution of 4 cm^{-1}, with 32 scans from 4000 to 500 cm^{-1}. Thermogravimetric analyses: Thermograms were made with a Mettler-Toledo TGA2 (Mettler Toledo, Greifensee, Switzerland), under nitrogen with a flow rate of 40 mL min^{-1}, using alumina pans. 5 to 10 mg of each sample were put in a standard TGA alumina crucible pan and heated from 30 °C to 600 °C at a heating rate of 10 °C/min.).

3.3. Compound 7

This compound has been reported before [35]. Herein we provide a variation of its method of preparation. Specifically, in a two-neck 50 mL dry round bottom flask (rbf) equipped with a magnetic bar was added 1.56 g of 4,4′-bipyridine (10 mmol) and was dissolved in 8 mL of freshly-distilled acetonitrile. The solution was brought to reflux (81 °C). To the refluxing solution of 4,4′-bipyridine a solution of 1.00 g (3.78 mmol) of 1,2-bis(bromomethyl)benzene in 10 mL of acetonitrile was added portion-wise within 30 min. The resulting reaction mixture was stirred under reflux for 2 h. During the first hour of the reaction a beige precipitate was already formed. The reaction mixture was allowed to cool down to r.t. and it was observed that more precipitate was formed during cooling. The solid was then filtered off by suction and was washed with cold ethanol and subsequently diethylether. The separated solid was purified as follows: the solid was then dried on the filter and then it was collected in an rbf where it was dissolved in 25 mL of warm water the (50 °C). The solution was filtered through Filtrox adapted on a sintered glass filter (porosity level 3) to remove undissolved material. The clear solution was then added dropwise in a beaker containing 200 mL of acetone and immediately a shiny beige precipitate was formed. Washing the solid with diethyl ether and subsequently Drying *in vacuo* at r.t. overnight resulted in 2.03 g of 7 (93 %). The product was used as it was obtained in the next step.

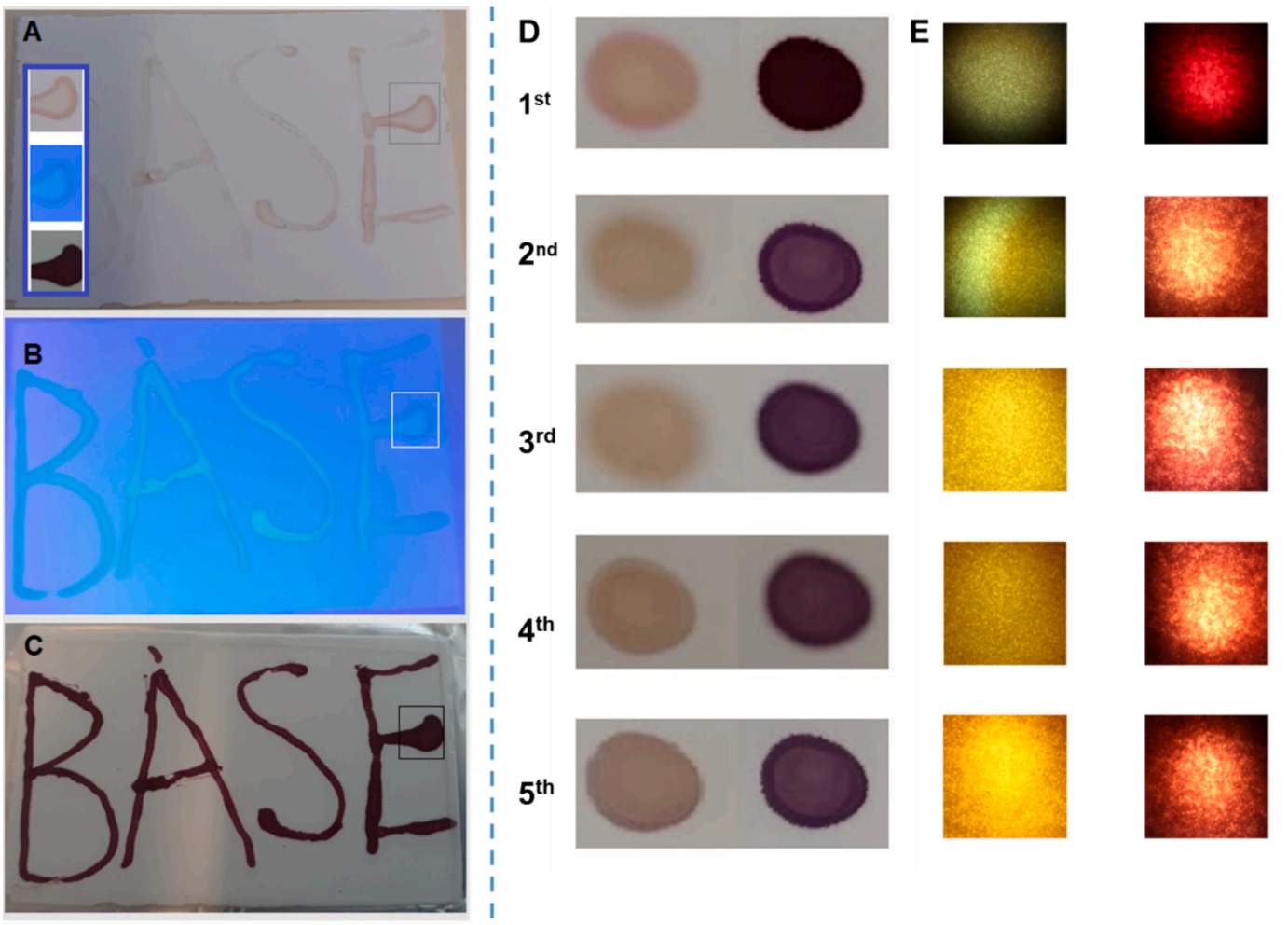

Fig. 12. Photos depicting a message written using $PABV_{aq}$ on the surface of a SiO_2-TLC plate recorded A) under ambient light prior to exposure to NH_3, B) UV-light ("black-light") prior to exposure to NH_3 and C) ambient light after exposure to NH_3. Inset in panel A depicts a detail monitored under the conditions A-C. D) Photos of **8** on SiO_2-TLC after 5 colaration/discoloration cycles E) Optical microscope images of **8** on SiO_2-TLC after 5 colaration/discoloration cycles.

3.4. Compound *8*

1.73 g (8.70 mmol) of phenacyl bromide was dissolved in 20 mL of dry DMF in a 50 mL rbf equipped with a magnetic bar. To this solution was added 1.00 g of **7** (1.74 mmol) and the mixture was heated at 80 °C and it was fully dissolved after a few minutes. The mixture darkened in color after the full dissolution of **7**. Heating at 80 °C was continued for 6 h. TLC was used to monitor the progress of the reaction. The mixture was then allowed to cool down to r.t. and it was then added to a beaker containing ethyl acetate (10 fold the reaction mix. Volume i.e. approx. 200 mL) while stirring. Immediately a shiny light yellow colored precipitate was formed. The stirring was continued for 10 min and then the precipitate was allowed to sediment. Filtration of the solid with suction through a porosity grade 3 fritted filter and washing with ethyl acetate and finally diethyl ether several times resulted in 1.25 g of **8** (74 %). The product was further purified by dissolving the product in 20 mL of distilled water and reprecipitating by adding it in 200 mL of absolute ethanol while stirring. Filtering and drying *in vacuo* resulted in purified **8** in 92 % purification yield (1.15 g of **8** was finally obtained). mp: 242 °C (decomp.); ^{1}H NMR (500 MHz, DMSO-d_6) $\delta = 9.60$ (*d*, $J = 6.26$ Hz, 4H; C_5H_4N), 9.39 (*d*, $J = 6.37$ Hz, 4H; C_5H_4N), 9.00 (*d*, $J = 6.41$ Hz, 4H; C_5H_4N), 8.96 (*d*, $J = 6.33$ Hz, 4H; C_5H_4N), 8.11 (*d*, $J = 7.32$ Hz, 4H; Ph_{PhAc}), 7.82 (*t*, $J = 7.31$ Hz, 2H, Ph_{PhAc}), 7.69 (*t*, $J = 7.89$ Hz, 4H, Ph_{PhAc}), 7.57 (*m*, 2H, Ph_{xyl}) 7.37 (m, 2H, Ph_{xyl}), 6.73 (s, 4H, $>CH_{2,PhAc}$), 6.48 (s, 4H, $>CH_{2,xyl}$); ^{13}C NMR (125 MHz, DMSO-d_6) 190.93, 163.54, 162.81, 149.84, 149.67, 147.69, 146.73, 135.33, 133.92, 133.24, 130.69, 130.22, 129.72, 129.06, 128.81, 127.75, 127.04, 67.17, 66.85. IR: $\tilde{\nu}$(C═O; ket.): 1696 cm^{-1}, (C═C; arom.): 1637 cm^{-1}, (C═N; pyrid.): 1558 cm^{-1}, (α-CH_2; PhAc): 1449 cm^{-1}; UV–Vis (DMSO) λ_{nm} (logε)): 564 (3.20); elemental analysis calcd (%) for: $C_{44}H_{56}N_4O_{11}Br_4$ ($C_{44}H_{38}N_4O_2Br_4{\cdot}9H_2O$) C: 45.77, H: 5.06, N:4.85, found: C: 45.65, H: 5.23, N:4.99; TGA: loss of ca. 9 molecules of H_2O upon heating.

3.5. Deprotonation of *8*

In a 10 mL rbf, 10 mg of **8** were dissolved in 5 mL of a 1/1 (v/v) ethanol/water mixture forming a 1.76 mM solution. To this solution under stirring 1 mg of NaOH dissolved in 1 mL of Milli-Q water was added and immediately the mixture was colored deep blue. The mixture was stirred for 10 min and then it was poured in a beaker containing 20 mL isopropanol. Immediately, a shiny blue precipitate was formed. The solid was filtered by suction and washed with small amount of cold ethanol and isopropanol. The solid was then dried *in vacuo* at 40 °C overnight and then it was analyzed through FTIR.

3.6. Staining of TLC plates

A freshly prepared 10 mM aqueous solution of PABV (Milli-Q water) was applied using a Pasteur pipette to a TLC SiO_2 plate (250 μm thickness; particle size 10–12 μm; pore size 60 Å). A message was written on

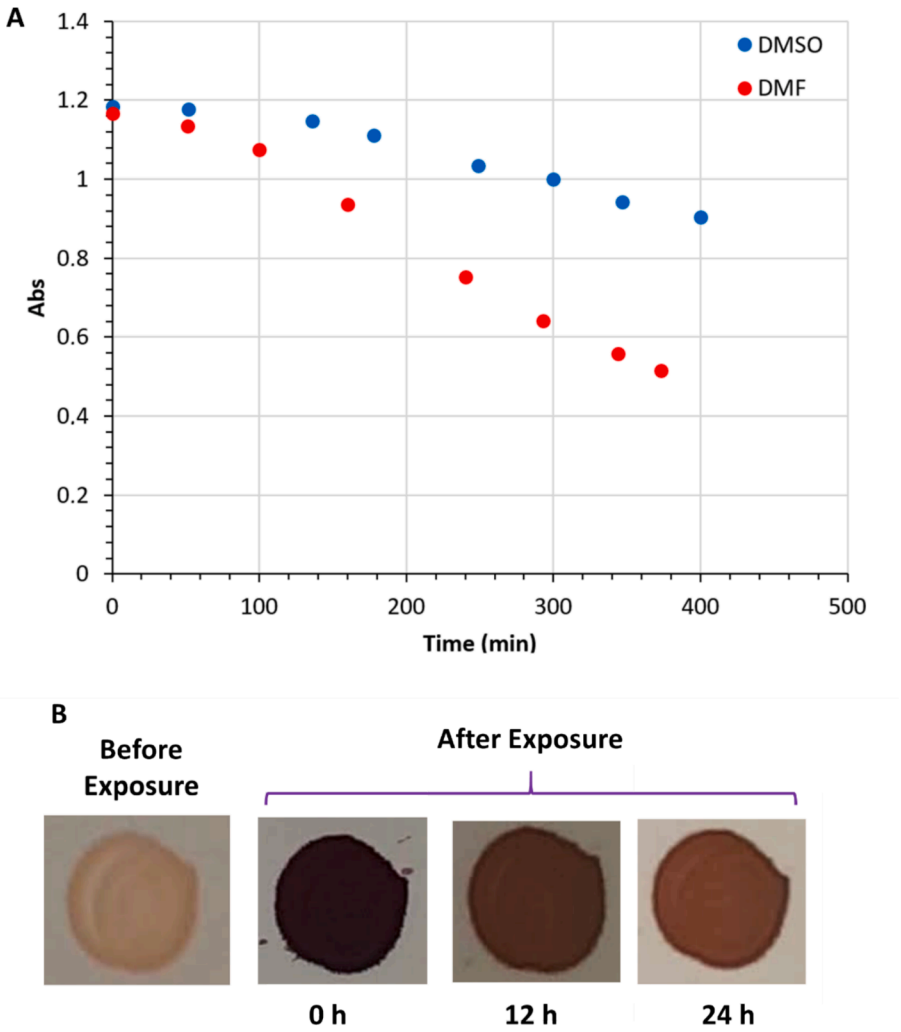

Fig. 13. A) Plot of the Absorbance of solutions of PABV in DMF and DMSO against time indicating stability of the solvent induced color over time. B) Photo of a SiO2-TLC stained with PABV before and after exposure to ammonia vapors at different time points.

the TLC plate, ensuring the solution was applied evenly and without causing any damage to the SiO_2 layer. The plate was allowed to dry at room temperature for 10 min using a stream of argon gas to facilitate water evaporation. Subsequently, the TLC plate was fixed to the lid of a 250 mL beaker, with the message facing the inside bottom of the beaker, which contained 2 mL of 28 % NH_4OH_{aq} solution. The color of the written message turned violet within seconds of attaching the lid. To test the reversibility of the chromic effect, the purple TLC plate after 5 min of exposure to ammonia, was placed in a 250 mL beaker containing 5 mL of 10 % HCl_{aq}. The process was slower; after 20 min, the message turned light brown/yellow, proving reversibility of the process.

*3.7. Vapochromism reversibility experiment of viologen **8***

On a SiO_2-TLC plate with absorbed viologen **8**, coloration was induced by exposing it to ammonia vapors for 10 s. Photos were taken with a regular camera as well as using an optical microscope under identical illumination conditions. The color was then reversed by exposing the viologen-on-TLC sample to HCl-vapors for 10 s, and photos were taken again in the same manner. This process was repeated five times to assess the reversibility of the vapochromism.

4. Conclusion

In addition to its intriguing color changes, PABV's pronounced sensitivity to both organic and inorganic bases holds significant promise for various applications. Understanding the interaction between PABV and bases—such as DIPEA—can inform the design of novel chemical sensors. By exploiting the specific response of PABV to different bases, the development of sensitive and selective detection methods can be enabled. Furthermore, the saturation behavior observed in the CT band at higher DIPEA concentrations suggests a potential limit of detection, which could be valuable for quantitative analysis. Future studies may explore PABV's behavior in different solvent environments, investigate other base-analyte interactions, and optimize its performance for practical sensing devices. Overall, PABV's unique properties make it an exciting candidate for advancing chemical sensing and analytical techniques.

CRediT authorship contribution statement

Valentin Silveira: Writing – review & editing, Visualization, Validation, Investigation. **Raffaello Papadakis:** Writing – review & editing, Writing – original draft, Visualization, Validation, Supervision, Resources, Project administration, Methodology, Investigation, Formal analysis, Conceptualization.

Declaration of competing interest

The authors declare that they have no known competing financial

interests or personal relationships that could have appeared to influence the work reported in this paper.

Acknowledgements

Prof. Emer. Dr. Athanase Tsolomitis (NTUA, Athens, Greece) is gratefully acknowledged for his invaluable comments and guidance over the years.

Data availability

No data was used for the research described in the article.

References

[1] R. Papadakis, Mono- and Di-quaternized 4,4'-bipyridine derivatives as key building blocks for medium- and environment-responsive compounds and materials, Molecules 25 (1) (2019) 1, https://doi.org/10.3390/molecules25010001.
[2] L. Striepe, T. Baumgartner, Viologens and their application as functional materials, Chemistry 23 (67) (2017) 16924–16940, https://doi.org/10.1002/chem.201703348.
[3] J. Ding, C. Zheng, L. Wang, C. Lu, B. Zhang, Y. Chen, M. Li, G. Zhai, X. Zhuang, Viologen-inspired functional materials: synthetic strategies and applications, J. Mater. Chem. A 7 (41) (2019) 23337–23360, https://doi.org/10.1039/c9ta01724k.
[4] X.-H. Zhou, Y. Fan, W.-X. Li, X. Zhang, R.-R. Liang, F. Lin, T.-G. Zhan, J. Cui, L.-J. Liu, X. Zhao, K.-D. Zhang, Viologen derivatives with extended π-conjugation structures: From supra-/molecular building blocks to organic porous materials. Zhongguo Hua Xue Kuai Bao, Chin. Chem. Lett. 31 (7) (2020) 1757–1767, https://doi.org/10.1016/j.cclet.2019.12.039.
[5] K. Madasamy, V.M. Shanmugam, D. Velayutham, M. Kathiresan, Reversible 2D supramolecular organic frameworks encompassing viologen cation radicals and CB, Sci. Rep. 8 (1) (2018) 1354, https://doi.org/10.1038/s41598-018-19739-7.
[6] A.K. Jeevan, K.R. Gopidas, Self-assembly and photochemistry of a pyrene-methyl viologen supramolecular fiber system, J. Phys. Chem. B 125 (30) (2021) 8539–8549, https://doi.org/10.1021/acs.jpcb.1c04417.
[7] Y.H. Ko, I. Hwang, H. Kim, Y. Kim, K. Kim, Molecular pop-up toy: a molecular machine based on folding/unfolding motion of alkyl chains bound to a host, Chem. Asian J. 10 (1) (2015) 154–159, https://doi.org/10.1002/asia.201402988.
[8] Wang, Y., Sun, J., Liu, Z., Nassar, M. S., Botros, Y. Y., & Stoddart, J. F. (2017). Radically promoted formation of a molecular lasso. Chemical Science (Royal Society of Chemistry: 2010), 8(4), 2562–2568. doi:10.1039/c6sc05035b.
[9] I. Deligkiozi, R. Papadakis, A. Tsolomitis, Synthesis, characterisation and photoswitchability of a new [2rotaxane of α-cyclodextrin with a diazobenzene containing π-conjugated molecular dumbbell, Supramol. Chem. 24 (5) (2012) 333–343, https://doi.org/10.1080/10610278.2012.660529.
[10] Q. Van Nguyen, T.P. Nguyen, H.T. Le, G. Le Truong, Volatile conductance switching in molecular device based on viologen building block, J. Phys. Chem. C. Nanomater. Interfaces 128 (33) (2024) 14118–14125, https://doi.org/10.1021/acs.jpcc.4c04567.
[11] S.-Z. Chang, H.-X. Zhong, Y.-H. Chen, Y.-H. Lin, F.-X. Wang, Y.-M. Fu, Q.-H. Pan, Multi-stimuli-responsive Chromic Switching Self-assembled with Polyoxometalate and Copper-viologen Frameworks, cMat (2) (2024) 1, https://doi.org/10.1002/cmt2.22.
[12] K.W. Shah, S.-X. Wang, D.X.Y. Soo, J. Xu, Viologen-based electrochromic materials: From small molecules, polymers and composites to their applications, Polymers 11 (11) (2019) 1839, https://doi.org/10.3390/polym11111839.
[13] P. Gao, Y. Pan, H. Han, Z. Gu, H. Chen, Z. Wu, H. Liu, S. Peng, X.-P. Zhang, R. Zhang, J. Liu, Molecular engineering of π-extended viologens consisting of thiophene-based bridges for electrochromic devices, J. Mol. Struct. 1288 (135769) (2023) 135769, https://doi.org/10.1016/j.molstruc.2023.135769.
[14] R. Papadakis, I. Deligkiozi, A. Tsolomitis, Synthesis and characterization of a group of new medium responsive non-symmetric viologens. Chromotropism and structural effects. Dyes and Pigments: An, Int. J. 95 (3) (2012) 478–484, https://doi.org/10.1016/j.dyepig.2012.06.013.
[15] R. Papadakis, The solvatochromic behavior and degree of ionicity of a synthesized pentacyano (N-substituted-4,4′-bipyridinium) ferrate(II) complex in different media. Tuning the solvatochromic intensity in aqueous glucose solutions, Chem. Phys. 430 (2014) 29–39, https://doi.org/10.1016/j.chemphys.2013.12.008.
[16] B. Wang, H. Tahara, T. Sagara, Enhancement of deformation of redox-active hydrogel as an actuator by increasing pendant viologens and adding filler or counter-charged polymer, Sens. Actuat. B Chem. 331 (129359) (2021) 129359, https://doi.org/10.1016/j.snb.2020.129359.
[17] S. Chandra, A. Lielpetere, W. Schuhmann, Designing a high-potential metal-free viologen-based redox polymer for effective wiring of FAD-dependent glucose dehydrogenase, Sens. Actuat. B Chem. 397 (134660) (2023) 134660, https://doi.org/10.1016/j.snb.2023.134660.
[18] F. Amir, X. Li, M.C. Gruschka, N.D. Colley, L. Li, R. Li, H.R. Linder, S.A. Sell, J. C. Barnes, Dynamic, multimodal hydrogel actuators using porphyrin-based visible light photoredox catalysis in a thermoresponsive polymer network, Chem. Sci. 11 (40) (2020) 10910–10920, https://doi.org/10.1039/d0sc04287k.
[19] M. Hu, F. Xing, Y. Zhao, Y.-L. Bai, M.-X. Li, S. Zhu, Phenolacetyl viologen as multifunctional chromic material for fast and reversible sensor of solvents, base, temperature, metal ions, NH3 vapor, and grind in solution and solid state, ACS Omega 2 (3) (2017) 1128–1133, https://doi.org/10.1021/acsomega.7b00035.
[20] R. Papadakis, A. Tsolomitis, Study of the correlations of the MLCT Vis absorption maxima of 4-pentacyanoferrate- 4′-arylsubstituted bispyridinium complexes with the Hammett substituent parameters and the solvent polarity parameters E and AN, J. Phys. Org. Chem. 22 (5) (2009) 515–521, https://doi.org/10.1002/poc.1514.
[21] I. Deligkiozi, E. Voyiatzis, A. Tsolomitis, R. Papadakis, Synthesis and characterization of new azobenzene-containing bis pentacyanoferrate(II) stoppered push–pull [2]rotaxanes, with α- and β-cyclodextrin. Towards highly medium responsive dyes, Dyes Pigm.: Int. J. 113 (2015) 709–722, https://doi.org/10.1016/j.dyepig.2014.10.005.
[22] I. Deligkiozi, R. Papadakis, Probing solvation effects in binary solvent mixtures with the use of solvatochromic dyes, In Dyes and Pigments - Novel Applications and Waste Treatment (2021), https://doi.org/10.5772/intechopen.98180.
[23] C. Gaina, V. Gaina, A. Airinei, E. Avram, Polyimides containing 4,4?-bipyridinium units, J. Appl. Polym. Sci. 94 (5) (2004) 2091–2100, https://doi.org/10.1002/app.21145.
[24] R. Papadakis, Preferential solvation of a highly medium responsive pentacyanoferrate(II) complex in binary solvent mixtures: Understanding the role of dielectric enrichment and the specificity of solute–solvent interactions, J. Phys. Chem. B 120 (35) (2016) 9422–9433, https://doi.org/10.1021/acs.jpcb.6b05868.
[25] Lothenbach, B., Durdziński, P., & De Weerdt, K. (2016). Thermogravimetric Analysis. In A Practical Guide to Microstructural Analysis of Cementitious Materials (1st ed., pp. 36). CRC Press. https://doi.org/10.1201/b19074-5.
[26] H. Greschonig, O. Glatter, Determination of equivalence points of sigmoidal potentiometric titration curves, Mikrochim. Acta 89 (1986) 401–409, https://doi.org/10.1007/BF01207332.
[27] C. Reichardt, Solvatochromic dyes as solvent polarity indicators, Chem. Rev. 94 (8) (1994) 2319–2358, https://doi.org/10.1021/cr00032a005.
[28] C. Reichardt, T. Welton, Solvents and Solvent Effects in Organic Chemistry, fourth ed., Wiley VCH Verlag GmbH & Co., Weinheim, Germany, 2011.
[29] V. Gutmann, Solvent effects on the reactivities of organometallic compounds, Coord. Chem. Rev. 18 (2) (1976) 225–255, https://doi.org/10.1016/s0010-8545(00)82045-7.
[30] T.M. Krygowski, W.R. Fawcett, Complementary Lewis acid-base description of solvent effects. I. Ion-ion and ion-dipole interactions, J. Am. Chem. Soc. 97 (8) (1975) 2143–2148, https://doi.org/10.1021/ja00841a026.
[31] R. Papadakis, Solute-centric versus indicator-centric solvent polarity parameters in binary solvent mixtures. Determining the contribution of local solvent basicity to the solvatochromism of a pentacyanoferrate(II) dye, J. Mol. Liq. 241 (2017) 211–221, https://doi.org/10.1016/j.molliq.2017.05.147.
[32] Y. Marcus, Solvent Mixtures: Properties and Selective Solvation, CRC Press, 2002.
[33] R.D. Williams, N.V. Yakhontov, Some aspects of the thermodynamics of mixtures of nonelectrolytes, Thermochim Acta 62 (1) (1983) 1–26, https://doi.org/10.1016/0040-6031(83)80080-X.
[34] W.L.F. Armarego, D.D. Perrin, Purification of Laboratory Chemicals, fourth ed., Butterworth-Heinemann, Oxford, 1988.
[35] W. Geuder, S. Hünig, A. Suchy, Single and double bridged viologens and intramolecular pimerization of their cation radicals, Tetrahedron (42) (1986) 1665–1677, https://doi.org/10.1016/S0040-4020(01)87583-9.